

Tertiary and quaternary solutions for plane Couette flow

By R. M. CLEVER¹ AND F. H. BUSSE²

¹Institute of Geophysics and Planetary Physics, University of California at Los Angeles,
CA 90024, USA

²Institute of Physics, University of Bayreuth, D-95440 Bayreuth, Germany

(Received 22 July 1996 and in revised form 4 March 1997)

The plane Couette system does not exhibit any secondary solutions bifurcating from the primary solution of constant shear. Since the work of Nagata (1990) it has been well known that three-dimensional steady solutions exist. Here the manifold of those steady solutions is explored in the parameter space of the problem and their instabilities are investigated. These instabilities usually lead to time-periodic solutions whose properties do not differ much from those of the steady solutions except that the amplitude varies in time. In some cases travelling wave solutions which are asymmetric with respect to the midplane of the layer are found as quaternary states of flow. Similarities with longitudinal vortices recently observed in experiments are discussed.

1. Introduction

Plane Couette flow represents the simplest solution of the Navier–Stokes equation of motion. But it has some unusual properties. Although the constant shear is known to be replaced by a turbulent state of flow at sufficiently high Reynolds numbers, theoretical analysis indicates that it is stable with respect to arbitrary infinitesimal disturbances. Nevertheless, steady solutions describing two-dimensional and three-dimensional flows exist even though they do not bifurcate from the basic solution of a plane shear. The three-dimensional solutions can be understood as tertiary solutions arising from secondary bifurcations if the plane Couette problem is imbedded in a more general problem. Nagata (1988, 1990) found the three-dimensional solutions through the consideration of higher bifurcations in the small-gap limit of the circular Couette problem in the special limit of vanishing mean rate of rotation in which case the problem turns out to be identical with the plane Couette problem. Clever & Busse (1992) found the same tertiary solution in the case of the Bénard–Couette problem of a fluid layer heated from below with the horizontal boundaries moving in opposite directions. The wavy roll solutions generated by the secondary bifurcation from longitudinal convection rolls persist in the isothermal limit of vanishing Rayleigh number which is identical with the plane Couette problem. In this paper the manifold of these solutions is more fully explored and further bifurcations leading to quaternary solutions are analysed.

Besides the three-dimensional steady solutions in the form of wavy longitudinal rolls two-dimensional steady finite-amplitude solutions have also been found recently (Cherhabili & Ehrenstein 1995) which do not depend on the spanwise coordinate.

These solutions describe flow in the form of spatially localized transverse rolls, but they require Reynolds numbers Re which are of the order 10 times higher than the minimum values of Re for the existence of the wavy roll solutions considered in the present paper. Most recently the same authors (Cherhabili & Ehrenstein 1996) have found three-dimensional versions of the localized rolls characterized by transverse modulations. Because of the large difference in the values of Re we have not yet been able to establish connections between the localized solutions and the spatially periodic solutions of the present analysis.

In the following the mathematical methods for the analysis of the problem will be described briefly in §2. Steady three-dimensional solutions in the form of wavy rolls will be discussed in §3. Their instabilities and the time-dependent periodic solutions that evolve from the steady states are studied in §4. The paper closes with a discussion section.

2. Mathematical formulation of the problem

We consider a layer of an incompressible fluid with thickness d bounded by two parallel rigid plates which move relative to each other with the velocity \hat{U} in the x -direction of a Cartesian system of coordinates. The z -coordinate is directed normal to the plates. Using d as length scale and d^2/ν as time scale, where ν is the kinematic viscosity of the fluid, we can write the basic Navier–Stokes equations in the form

$$\frac{\partial}{\partial t} \mathbf{u} + \mathbf{u} \cdot \nabla \mathbf{u} = -\nabla \pi + \nabla^2 \mathbf{u} \quad (1a)$$

$$\nabla \cdot \mathbf{u} = 0. \quad (1b)$$

The boundary conditions are given by

$$\mathbf{u} = \pm \mathbf{i} Re/2 \quad \text{at} \quad z = \pm \frac{1}{2} \quad (2)$$

where \mathbf{i} is the unit vector in the x -direction and $Re = \hat{U}d/\nu$ is the Reynolds number. It is convenient to introduce the general representation for a solenoidal velocity field

$$\mathbf{u} = \mathbf{U}(z, t) + \nabla \times (\nabla \times \mathbf{k} \varphi) + \nabla \times \mathbf{k} \psi \equiv \mathbf{U} + \delta \varphi + \epsilon \psi \quad (3)$$

where \mathbf{k} is the unit vector in the z -direction and the condition that the average of φ and ψ over the (x, y) -plane vanishes can be imposed,

$$\bar{\varphi} = \bar{\psi} = 0, \quad \bar{\mathbf{u}} = \mathbf{U}(z, t) = (U_x, U_y, 0).$$

The equations for φ and ψ can be obtained in the form of the z -components of the curl curl and of the curl of equation (1a), respectively

$$\nabla^4 \Delta_2 \varphi = \mathbf{k} \cdot \nabla \times [\nabla \times (\delta \varphi + \epsilon \psi) \cdot \nabla (\delta \varphi + \epsilon \psi)] + \left(\mathbf{U} \cdot \nabla + \frac{\partial}{\partial t} \right) \nabla^2 \Delta_2 \varphi - \mathbf{U}'' \cdot \nabla \Delta_2 \varphi, \quad (4a)$$

$$\nabla^2 \Delta_2 \psi = -\mathbf{k} \cdot \nabla \times [(\delta \varphi + \epsilon \psi) \cdot \nabla (\delta \varphi + \epsilon \psi)] - \mathbf{U}' \cdot \epsilon \Delta_2 \varphi + \left(\mathbf{U} \cdot \nabla + \frac{\partial}{\partial t} \right) \Delta_2 \psi, \quad (4b)$$

where Δ_2 denotes the two-dimensional Laplacian, $\Delta_2 = \partial^2/\partial x^2 + \partial^2/\partial y^2$, and where the primes denote differentiation with respect to z . The equation for \mathbf{U} is given by

$$\left(\partial_{zz}^2 - \frac{\partial}{\partial t} \right) \mathbf{U} = -\partial_z (\overline{\Delta_2 \varphi (\nabla_2 \varphi' + \epsilon \psi)}) \quad (4c)$$

where ∇_2 is the two-dimensional gradient, $\nabla_2 = \nabla - \mathbf{k}\partial/\partial z$. For the solution of equations (4) the Galerkin method will be employed. The dependent variables are expanded in complete systems of functions satisfying the respective boundary conditions,

$$\varphi = \sum_{l,m,n} a_{lmn}(t) \exp\{il\alpha_x x + im\alpha_y y\} g_n(z), \quad (5a)$$

$$\psi = \sum_{l,m,n} c_{lmn}(t) \exp\{il\alpha_x x + im\alpha_y y\} \sin n\pi(z + \frac{1}{2}), \quad (5b)$$

$$\mathbf{U} = Re z \mathbf{i} + \sum_n (U_n(t) \mathbf{i} + V_n(t) \mathbf{j}) \sin n\pi(z + \frac{1}{2}), \quad (5c)$$

where the Chandrasekhar (1961) functions $g_n(z)$ are defined by

$$g_n = \frac{\cosh \lambda_n z}{\cosh \lambda_n \frac{1}{2}} - \frac{\cos \lambda_n z}{\cos \lambda_n \frac{1}{2}} \text{ for odd } n, \quad g_n = \frac{\sinh \lambda_n z}{\sinh \lambda_n \frac{1}{2}} - \frac{\sin \lambda_n z}{\sin \lambda_n \frac{1}{2}} \text{ for even } n, \quad (6a)$$

and the numbers λ_n are determined such that the conditions $g'(z) = g(z) = 0$ at $z = \pm \frac{1}{2}$ are satisfied,

$$\tanh \frac{1}{2} \lambda_n + \tan \frac{1}{2} \lambda_n = 0 \text{ for odd } n, \quad \coth \frac{1}{2} \lambda_n - \cot \frac{1}{2} \lambda_n = 0 \text{ for even } n. \quad (6b)$$

In order that real expressions (5a), (5b) are obtained, the conditions $a_{lmn} = a_{-l-mn}^*$, $c_{lmn} = c_{-l-mn}^*$ must be imposed where the asterisk indicates the complex conjugate. After representations (5) have been inserted into (4) and these are multiplied by the expansion functions and averaged over the fluid layer, a system of ordinary differential equations in time is obtained for the coefficients a_{lmn} , c_{lmn} , U_n and V_n . These equations can be solved after a truncation scheme has been established. We shall neglect all coefficients and corresponding equations for which

$$l + m + n \geq N_T \quad (7)$$

holds, where N_T is a natural number which will be chosen sufficiently high such that the physically significant properties of the solution change only minutely when N_T is replaced by $N_T + 2$.

Among the solutions those with constant coefficients a_{lmn} , c_{lmn} , U_n are of special interest since they can be obtained as solutions of an algebraic system of equations through the use of a Newton–Raphson method. The coefficients V_n vanish for these steady solutions. The stability of the steady three-dimensional solutions can then be studied through the superposition of infinitesimal disturbances of the form

$$\tilde{\varphi} = \exp\{idx + iby + \sigma t\} \sum_{l,m,n} \tilde{a}_{lmn} \exp\{il\alpha_x x + im\alpha_y y\} g_n(z), \quad (8a)$$

$$\tilde{\psi} = \exp\{idx + iby + \sigma t\} \sum_{l,m,n} \tilde{c}_{lmn} \exp\{il\alpha_x x + im\alpha_y y\} \sin m\pi(z + \frac{1}{2}). \quad (8b)$$

When (4a, b) are linearized in the disturbances $\tilde{\varphi}$, $\tilde{\psi}$ a homogeneous system of linear algebraic equations for the unknown coefficients \tilde{a}_{lmn} , \tilde{c}_{lmn} is obtained with the growth rate σ as eigenvalue. Whenever there exists a σ with positive real part as a function of b and d for a given steady solution of the form (5) with constant coefficients a_{lmn} , c_{lmn} , U_n , then the latter is regarded as unstable. Otherwise it will be considered as stable. There is no need to consider a disturbance of the mean flow since the right-hand side of (4c) vanishes when the terms linear in $\tilde{\varphi}$, $\tilde{\psi}$ are considered as long as d or

b is finite. In fact the disturbances of the mean flow are included in the representation (8a, b) where the sum includes the case $l = m = 0$ in contrast to the summation in (5a, b). Only in the special case $d = b = 0$ must the mean flow disturbance

$$\tilde{U} = \exp\{\sigma t\} \sum_n (\tilde{U}_n \mathbf{i} + \tilde{V}_n \mathbf{j}) \sin n\pi(z + \frac{1}{2}) \quad (8c)$$

be included in the stability analysis while the coefficients with subscripts $l = m = 0$ are dropped in (8a, b).

3. Steady three-dimensional solutions

In the Bénard–Couette problem longitudinal rolls are the preferred solution bifurcating from the basic solution in the form of a constant shear when the Rayleigh number Ra exceeds the critical value, $Ra_c = 1708$. When the Rayleigh number is increased, the longitudinal rolls become unstable to wavy disturbances provided the Reynolds number Re exceeds a critical value. Steady solutions in the form of wavy rolls bifurcate from the two-dimensional secondary solution. This bifurcation is supercritical if the Reynolds number is not too high, but for increasing values of Re the bifurcation becomes subcritical (Clever & Busse, 1992). For Reynolds numbers of the order 500 and higher the wavy roll solutions extend to $Ra = 0$ and to negative values of Ra . The wavy roll solutions can be represented in the form (5) with constant coefficients a_{lmn}, c_{lmn} which exhibit the following symmetry properties:

$$a_{lmn} = (-1)^{m+n} a_{-lmn}, \quad a_{lmn} = (-1)^l a_{l-mn}, \quad (9a)$$

$$c_{lmn} = (-1)^{m+n} c_{-lmn}, \quad c_{lmn} = -(-1)^l c_{l-mn}. \quad (9b)$$

Two typical examples of steady wavy roll solutions are shown in figure 1(a, b, c). The form of the solutions exhibits remarkably little variation with the parameters Re, α_x, α_y . As must be expected for a subcritically bifurcating solution there is an upper and a lower branch. Even though the amplitude of motion is much higher on the upper branch than on the lower branch, the spatial dependence is rather similar. As has already been discussed by Clever & Busse (1992) the waviness of the flow pattern is more pronounced near the boundaries, while in the midplane the rolls are rather straight except for sharp kinks as shown in figure 1(a). The lines of equal z -velocity u_z in plane $z = 0.4$ can be obtained from the lines in the plane $z = -0.4$ shown in figure 1(a) through the use of the symmetry property

$$u_z(x, y, z) = -u_z\left(\frac{2\pi}{\alpha_x} - x, \frac{\pi}{\alpha_y} + y, -z\right) \quad (9c)$$

which represents another way of expressing the left-hand conditions of property (9). The waviness of the longitudinal rolls manifests itself in the sidewise shifting of the plumes of positive and negative x -momentum shown in figure 1(b). The combined effect of longitudinal waviness and shearing is most strongly expressed by the lines of constant spanwise velocity shown in figure 1(c). The concentration of the mean shear towards the boundaries is quite evident from the plots of figure 1(c) as well as those of figure 1(b).

The physical quantity that best characterizes solutions of the plane Couette problem is the shear Nusselt number S which denotes the average viscous force exerted at the boundary divided by the same force in the case of the primary solution of constant shear. S is always equal to or larger than unity under stationary conditions. The

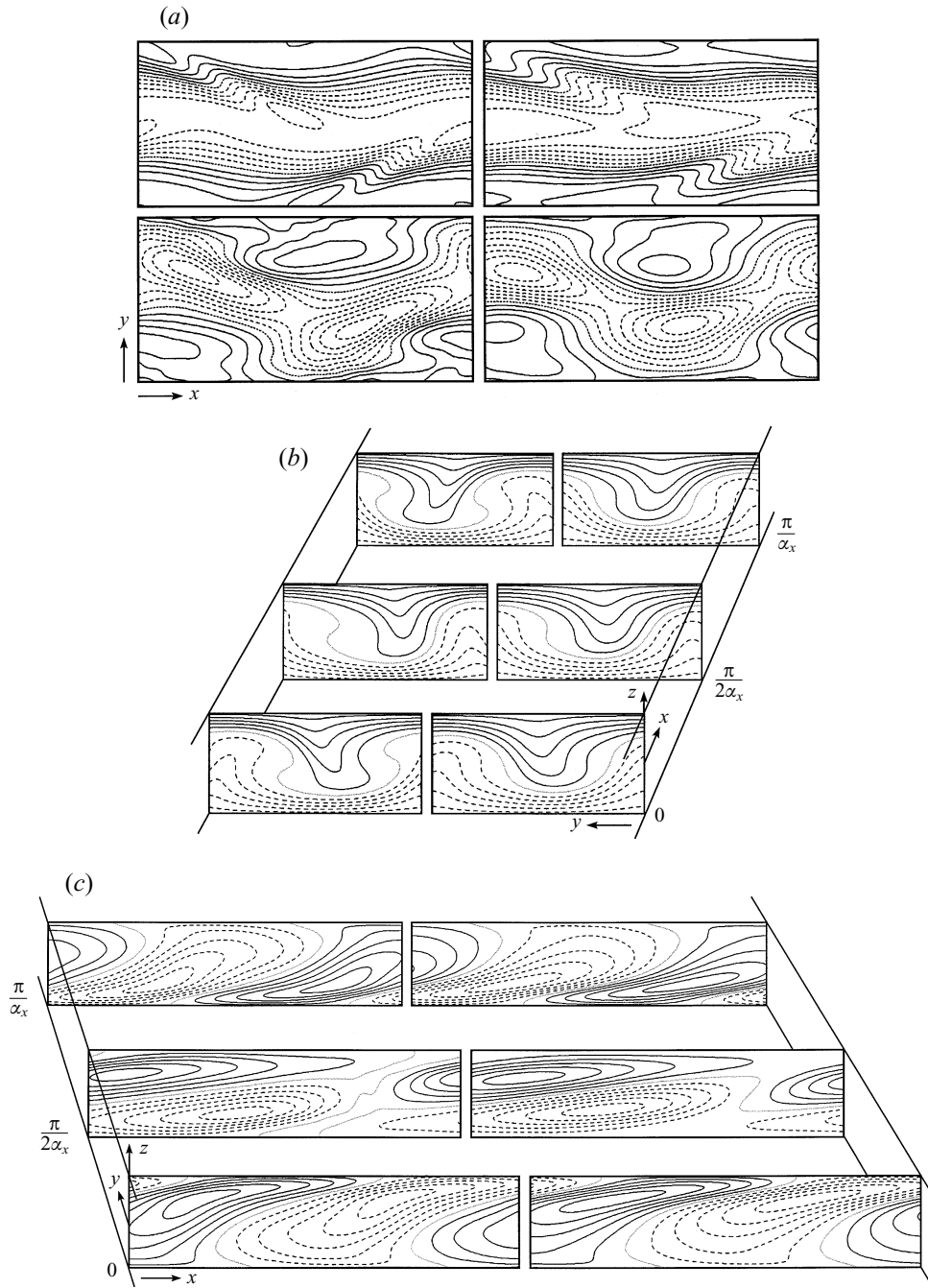


FIGURE 1. (a) Lines of constant z -velocity in the planes $z = 0$ (upper plots) and $z = -0.4$ (lower plots) in the cases of the upper branch (left plots) and of the lower branch (right plots). (b) Lines of constant x -velocity in the planes $x = 0, x = \pi/2\alpha_x, x = \pi/\alpha_x$ in the cases of the upper (left plots) and lower (right plots) branches. (c) Lines of constant y -velocity in the planes $y = 0, y = \pi/2\alpha_y, y = \pi/\alpha_y$ in the cases of the upper (left plots) and lower (right plots) branches. $Re = 600, \alpha_x = 1.5, \alpha_y = 3.0$. Solid lines indicate positive values, dashed lines negative.

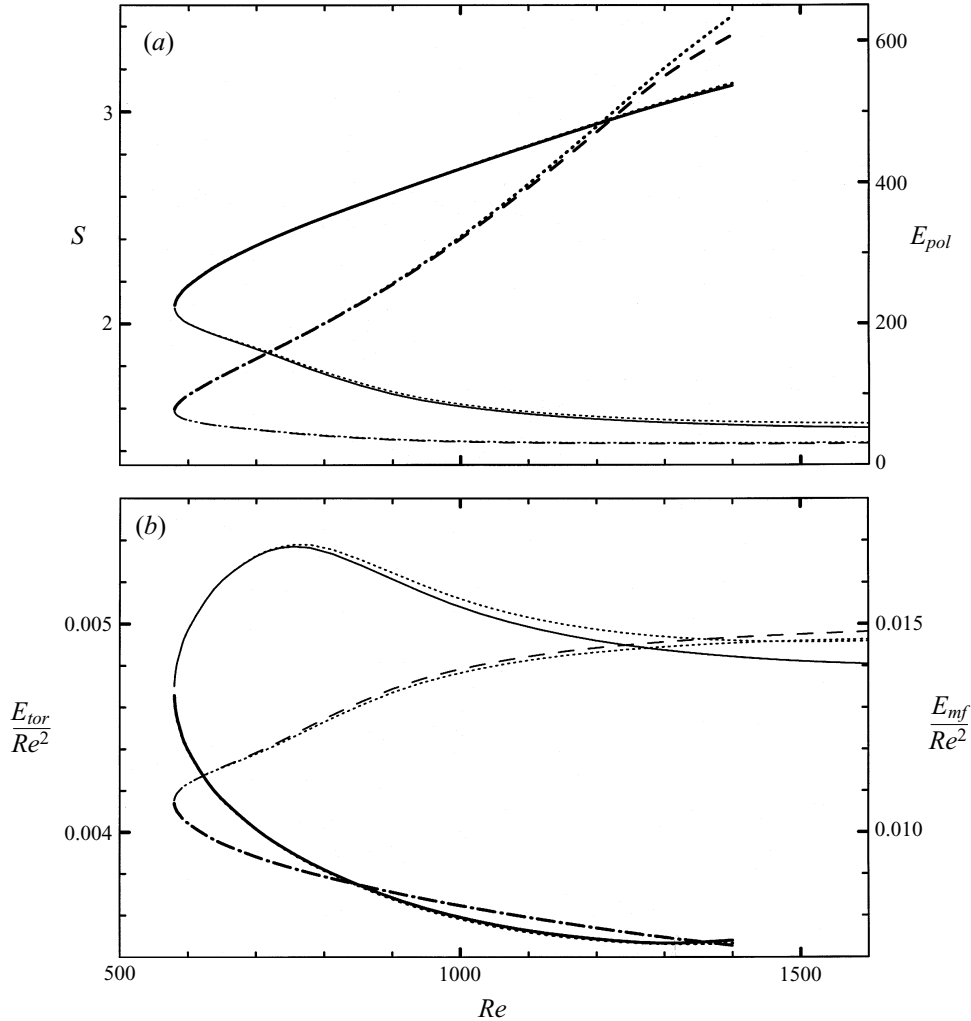


FIGURE 2. (a) The shear Nusselt number S (solid line) and the poloidal kinetic energy E_{pol} (dashed line) as a function of Re for wavy roll solutions with $\alpha_x = 1.5, \alpha_y = 2.5$. The upper branch is distinguished from the lower branch by a thicker line. The computations have been carried out for $N_T = 20$. Results obtained for $N_T = 18$ are shown by the dotted lines for comparison. (b) The same plot as (a) but for the toroidal kinetic energy E_{tor} (solid line) and the mean flow energy E_{mf} (dashed line).

dependence of S on Re for given values of α_x and α_y of the steady wavy rolls is shown in figure 2(a) with its upper and lower branches. The same dependence on Re is shown by the kinetic energy of the poloidal part of the motion

$$E_{pol} = \frac{1}{2} \langle |\nabla \times (\nabla \times \mathbf{k}\varphi)|^2 \rangle \quad (10)$$

in figure 2(a), while the kinetic energy of the toroidal part of the motion

$$E_{tor} = \frac{1}{2} \langle |\nabla \times \mathbf{k}\psi|^2 \rangle \quad (11)$$

and the kinetic energy of the mean flow as displayed in figure 2(b) show an inverted dependence, i.e. the lower-branch solution now corresponds to the high values while the values for the upper branch reside below. Since the roll-like motions derive their

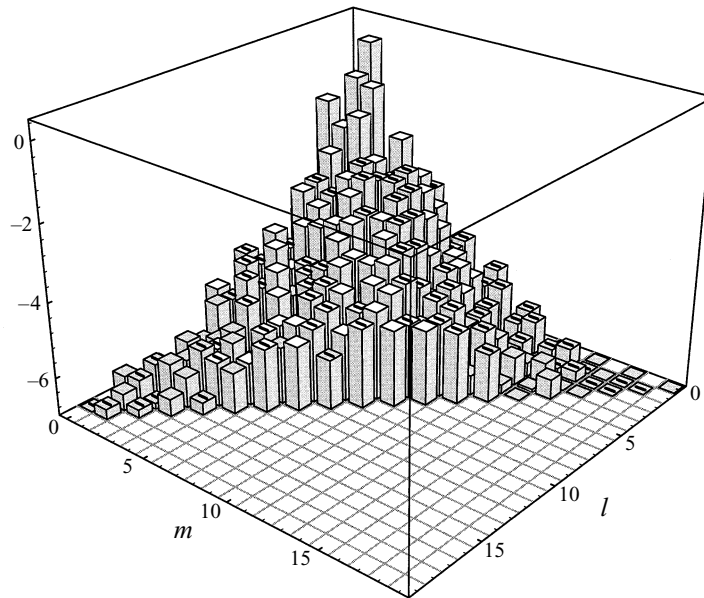


FIGURE 3. The logarithm of the absolute value of the coefficients a_{lm1} as a function of l and m in the case of the upper-branch solution with $Re = 10^3$, $\alpha_x = 1.5$, $\alpha_y = 2.5$. Negative coefficients are indicated by a minus sign on top of the columns.

energy from the mean flow, the energy of the latter is anticorrelated with E_{pol} . The toroidal component of motion is generated by the advection of the mean flow and thus decreases when the mean shear decreases in the interior of the layer.

In order to indicate the quality of the numerical approximation two different truncation parameters have been used for all curves of figure 2(a, b). Although the increase from 18 to 20 of the truncation parameter may appear to be small, it should be noted that the number of coefficients increases by more than one third from 1956 to 2680. Only for values of Re above 10^3 may the difference between the curves reach 1% or more. For this reason most of the detailed analysis of this paper will be carried out for values of Re less than 10^3 . To give a visual impression of the decay of the magnitude of coefficients, a_{lm1} have been plotted in figure 3 on a logarithmic scale for a solution with $N_T = 20$. A difference of more than four orders of magnitude can be seen between the largest coefficients and those at the truncation boundary.

To get a better picture of the dependence of S , E_{pol} and E_{tor} on the wavenumbers α_x and α_y of the wavy rolls, the variations of S , E_{tor} and E_{pol} with α_y are indicated for a set of different Reynolds numbers in figure 4(a-c). The curves shown in this figure are actually closed, but the numerical scheme used for the computations did not produce converging solutions in regions of very rapid change with α_y . The dependence of S on Re and α_y for a given α_x thus gives rise to a tube-like surface in the parameter space. The toroidal energy (11) measures mainly the spanwise variation of the x -component of the velocity field. It thus reaches a maximum for relatively low values of α since viscous stresses damp the variations in the y -direction for higher values of α_y . The dependence on α_x and Re for a fixed value of α_y corresponds to a similar tube-like surface as shown in figure 5.

Of particular interest is the lowest Reynolds number for which steady tertiary solutions can exist. The computations have therefore been extended over a broad

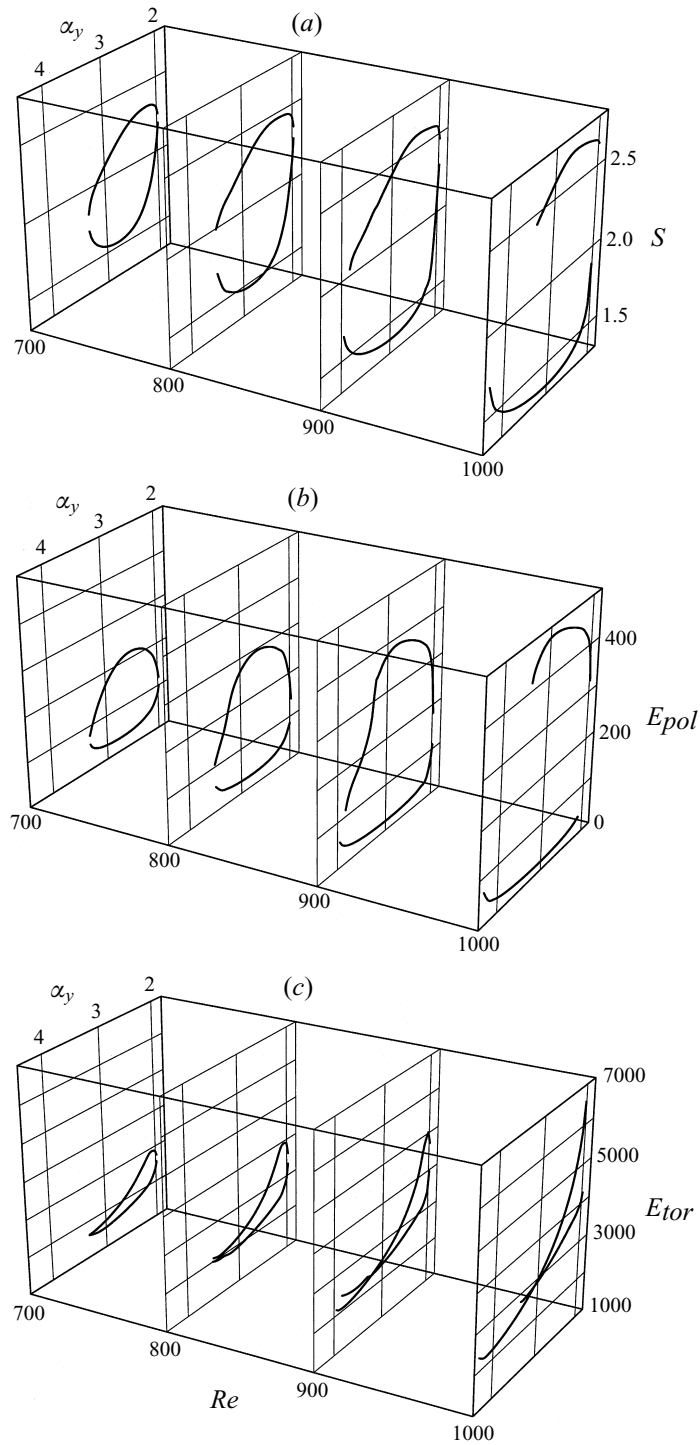


FIGURE 4. The shear Nusselt number S as a function of (a) α_y , (b) the poloidal energy E_{pol} , (c) the toroidal kinetic energy E_{tor} , for fixed $\alpha_x = 1.2$ at different values of Re as indicated.

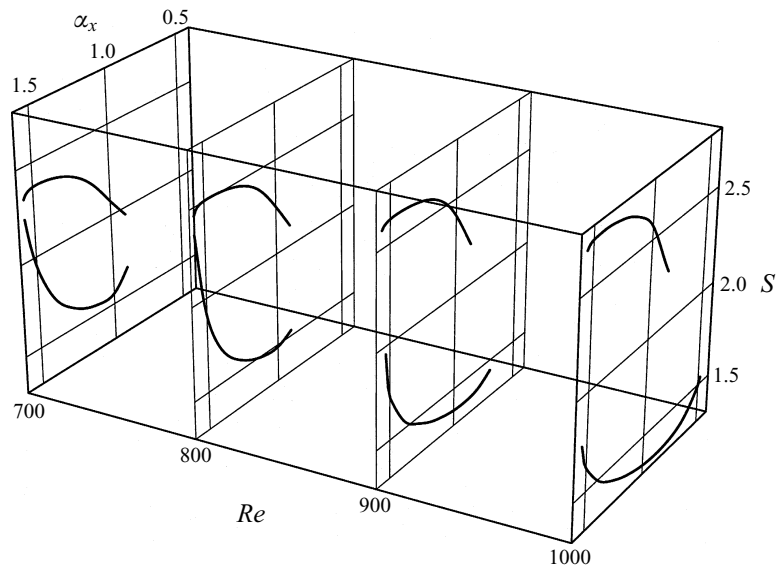


FIGURE 5. The shear Nusselt number S as a function of α_x for fixed $\alpha_y = 2.5$ at different values of Re as indicated.

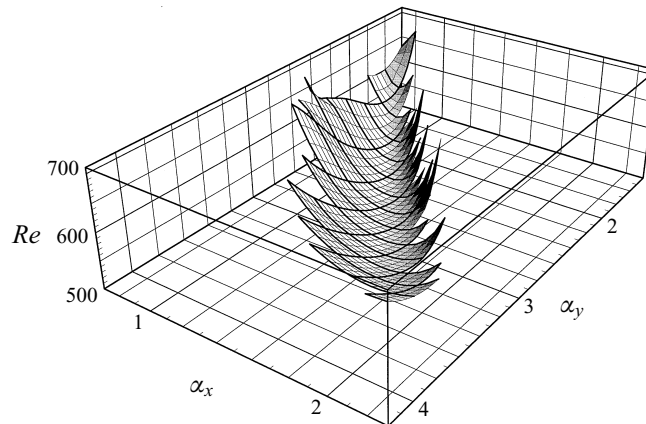


FIGURE 6. The minimum Reynolds number Re for the existence of steady wavy roll solutions as a function of the wavenumbers α_x and α_y .

range of wavenumbers α_x and α_y and the results for the lowest value of Re have been plotted in figure 6. It is evident that there exists a rather flat minimum which extends roughly along the line $\alpha_y \approx 2\alpha_x$.

4. Quaternary solutions bifurcating from tertiary solutions

It had already been shown by Clever & Busse (1992) that all wavy roll solutions of the branches that extend to the isothermal case of the plane Couette problem are unstable. Later computations by Nagata (1993) have extended these calculations by considering the stability with respect to subharmonic disturbances for a particular set of wavenumbers α_x, α_y of the steady wavy roll solution. In carrying out the stability analysis Clever & Busse have restricted the disturbances to those which fit

		Growth rates σ with maximum real part in the cases					
	<i>Re</i>	α_x	α_y	<i>SS</i>	<i>SA</i>	<i>AS</i>	<i>AA</i>
Upper branch	525	1.0	2.0	$-1.23 \pm i14.4$	-5.25	-6.78	$-16.4 \pm i18.6$
	540	1.0	2.0	$0.19 \pm i20.4$	-5.02	-6.87	-18.0
	600	1.0	2.5	$1.29 \pm i32.5$	-3.94	-7.45	-2.96
	540	1.5	3.0	$-7.3 \pm i5.0$	-4.03	-7.50	-13.6
	580	1.5	3.0	$0.48 \pm i40.4$			
	630	1.5	3.5	$-0.11 \pm i49.8$	-1.32	-8.63	
	670	1.5	3.5	$7.26 \pm i54.4$	0.15	-9.35	
	610	2.0	3.5	$-6.96 \pm i45.4$	-2.26	-8.39	-7.65
	640	2.0	3.5	$0.47 \pm i45.1$	-1.51	-8.99	-4.55
	675	1.0	3.0	$-3.3 \pm i35.0$		10.6	$-7.1 \pm i14.6$
Lower branch	520	1.0	2.0	7.17	-5.52	-6.65	$-13.7 \pm i18.2$
	540	1.0	2.0	13.2	-5.59	-6.52	$-11.8 \pm i18.0$
	565	1.0	2.0	9.37	-5.37	-6.49	$-15.0 \pm i18.3$
	600	1.0	2.5	14.4	-5.52	-6.35	$-12.8 \pm i18.2$
	540	1.5	3.0	5.99	-4.34	-7.28	-17.0
	560	1.5	3.0	13.7	-4.72	-6.91	-20.7
	595	2.0	3.5	6.55	-3.39	-7.64	-14.1

TABLE 1. Selected growth rates for disturbances of different symmetry classes

the periodicity interval $0 \leq x < 2\pi/\alpha_x$, $0 \leq y < 2\pi/\alpha_y$. In other words, the Floquet parameters b and d in (7) are assumed to vanish. This restriction permits an enormous simplification of the stability analysis in that for $d = b = 0$ the disturbances separate into four classes depending on whether they satisfy the symmetry conditions (9a) or their counterparts,

$$SS : \tilde{a}_{lmn} = (-1)^{m+n} \tilde{a}_{-lmn}, \quad \tilde{a}_{lmn} = (-1)^l \tilde{a}_{l-mn}, \tag{12a}$$

$$SA : \tilde{a}_{lmn} = (-1)^{m+n} \tilde{a}_{-lmn}, \quad \tilde{a}_{lmn} = (-1)^{l+1} \tilde{a}_{l-mn}, \tag{12b}$$

$$AS : \tilde{a}_{lmn} = (-1)^{m+n+1} \tilde{a}_{-lmn}, \quad \tilde{a}_{lmn} = (-1)^l \tilde{a}_{l-mn}, \tag{12c}$$

$$AA : \tilde{a}_{lmn} = (-1)^{m+n+1} \tilde{a}_{-lmn}, \quad \tilde{a}_{lmn} = (-1)^{l+1} \tilde{a}_{l-mn}. \tag{12d}$$

Analogous relationships based on the symmetries (9b) apply to the coefficients \tilde{c}_{lmn} . The stability analysis of the steady wavy roll solution with respect to the four disturbance classes (12) has been extended in the α_x, α_y, Re -parameter space. Some typical growth rates σ are given in table 1. As expected the lower-branch solutions are always unstable with respect to the *SS*-disturbances which exhibit the same symmetry as the steady states. The upper-branch solutions are also usually unstable except for a small range of Reynolds numbers just above the minimum value for which they can exist. Typically the most dangerous disturbances are again those with the same symmetry as the steady solution. But in contrast to disturbances on the lower branch the *SS*-disturbances on the upper branch usually correspond to an oscillatory onset of instability. In table 2 typical values are given of the frequency σ_i of oscillation at the onset of *SS*-disturbances. But there are examples of the *AS*-type instability preceding the onset of the *SS*-disturbances. Usually such cases correspond to wavenumbers of the steady solutions close to the boundary of its existence as in the case $\alpha_x = 1.0, \alpha_y = 3.0$ of table 1.

The oscillatory wavy roll solutions bifurcating from the steady wavy roll solutions in

α_x	α_y	Re_{min}	Re_{III}	σ_i
1.0	2.0	519	538	20
1.0	2.5	558	595	27
1.0	3.0	675	685	34
1.5	3.0	543	575	39
1.5	3.5	617	631	50
2.0	3.5	596	638	45

TABLE 2. Onset Reynolds number Re_{III} and frequency σ_i of the *SS*-instability of steady wavy rolls on the upper branch (Re_{min} gives an approximate lower bound for existence of the steady solution)

the form of *SS*-disturbances can be determined numerically relatively easily through a forward integration in time of the system of ordinary differential equations for the coefficients $a_{lmm}(t)$ and $c_{lmm}(t)$ as discussed in §2. Typical dependences on time of the energy of the fluctuating parts of the motion are shown in figure 7(*a, b*). The periods of oscillation agree quite well with those predicted on the basis of the stability analysis. For example the period $2\pi/\sigma_i$ given in table 2 for $\alpha_x = 1.0, \alpha_y = 2.5$ is within 10% of the period shown by the finite-amplitude oscillations displayed in figure 7. The oscillations seem to correspond to a periodic swinging back and forth between the steady states of the upper and the lower branches. The energies do not quite reach the extreme values marked by the steady states. But the amplitude of the oscillation increases just as the difference between the amplitudes on the upper and the lower branches increases with Re . The structure of the oscillatory wavy roll motion changes remarkably little throughout the cycle as is evident from the plots shown in figure 8. Although the amplitude changes by at least a factor of two, the motion remains very similar to the motion of steady wavy rolls as shown in figure 1(*a*). Since the maximum of the amplitude of motion is assumed close to $t = 0$ in the case of figure 8 it is not surprising that the pattern at $t = 0$ is nearly identical to that of the upper branch shown on the left-hand side of figure 1(*a*), while at later times in the cycle it changes in the direction of the pattern of the lower branch.

As the Reynolds number increases, a doubling of the period can often be observed as shown in the case of figure 7. But this doubling does not indicate the beginning of a period doubling sequence since a transition to aperiodic flow was usually found with maxima and minima following in an apparently irregular way. The changes of the mean profile of the flow through the cycles of oscillatory wavy rolls are relatively small. In figure 9 the variation of the mean flow component $U(z, t)$ in the x -direction is indicated for a case where E_{pol} varies by more than 50% from its mean value. There is a phase lag of nearly 90° between the maximum of E_{pol} and the maximal distortion of the mean flow profile from its linear shape in the plane Couette flow limit. After the E_{pol} has reached a maximal value, the transport of x -momentum leads to a maximum distortion which in turn decreases the mean flow energy which is available as the source for the poloidal component of motion. Only after the distortion has decayed does the fluctuating component of motion grow again in order to start a new cycle of oscillation. The energy of the toroidal component of motion is nearly opposite in phase to E_{pol} . This indicates that the oscillation can be understood in part as a periodic shift of the kinetic energy between poloidal and toroidal components.

The forward integration in time in the case of growing disturbances with the symmetry (12*c*) requires a considerably larger numerical effort since the number of coefficients doubles. A point of bifurcation of the *AS*-disturbances from the steady

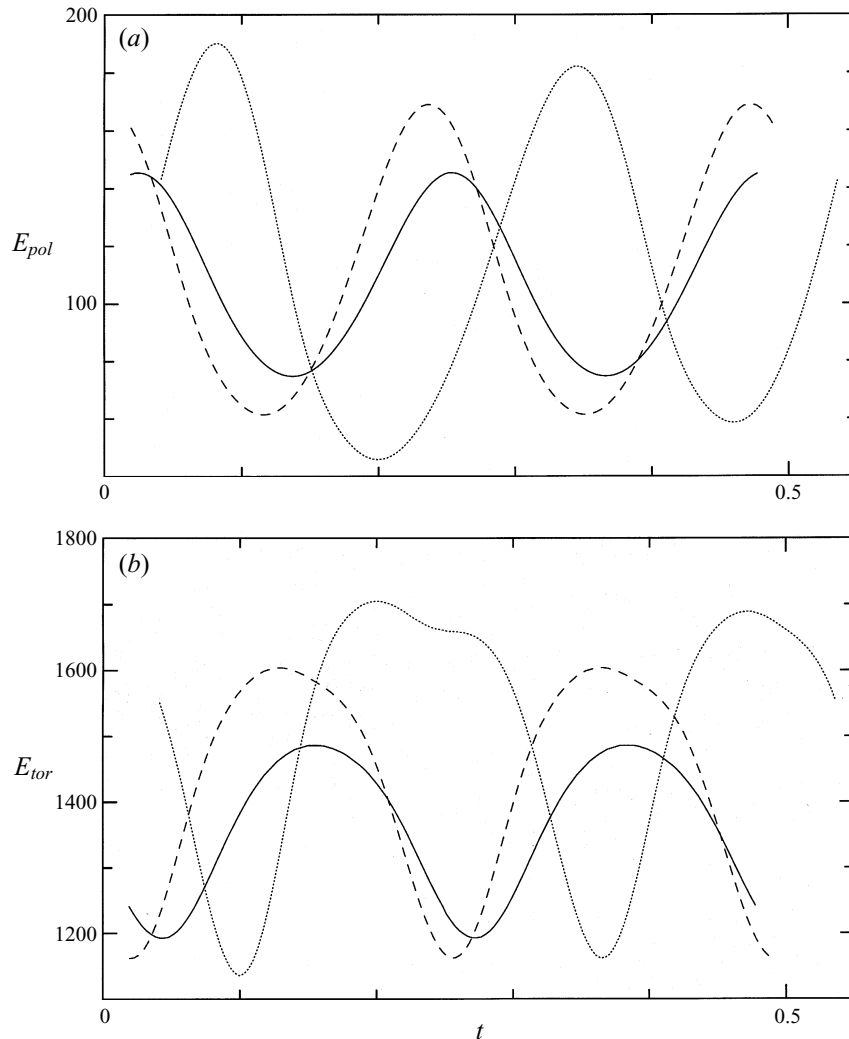


FIGURE 7. Time dependence of (a) E_{pol} and (b) E_{tor} for oscillatory wavy rolls with $\alpha_x = 1.0, \alpha_y = 2.5$ for the Reynolds numbers $Re = 610$ (solid curve), 620 (dashed curve), and 630 (dotted curve). Two periods are shown for $Re = 610, 620$, but only one period for $Re = 630$ since a period doubling occurs in the interval $620 < Re < 630$.

upper-branch solution with wavenumbers in the neighbourhood of $\alpha_x = 1.0, \alpha_y = 3.0$ could not be found since the steady solution ceased to exist towards lower values of Re before the growth rate of the AS -disturbances decreased to zero. But in following the evolution of the AS -disturbances through forward integrations in time, shape-preserving travelling wave solutions have been found. A comparison between these new solutions and the steady wavy roll solutions is shown in figures 10(a) and 10(b). The travelling wave solution is asymmetric with respect to the midplane of the layer which is apparent from figure 10(b). It also violates the symmetry property (9(c)) as can be seen from the asymmetry between ascending and descending motion in figure 10(a). There are always two asymmetric travelling wave (ATW) solutions differing in the sign of the coefficients with the symmetry property (12c). The mean flow profile

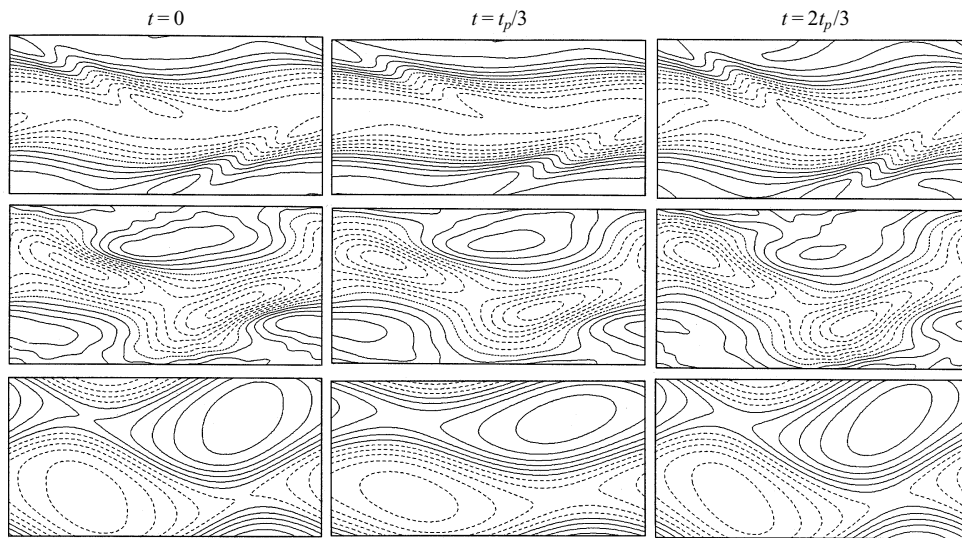


FIGURE 8. Lines of constant z -velocity in the planes $z = 0$ (upper row) and $z = -0.4$ (middle row), and lines of constant $\psi(x, y)$ in the plane $z = 0$ (lower row), in the case $\alpha_x = 1.5, \alpha_y = 3.0, Re = 600$ of the oscillatory wavy roll solution. The period of oscillation is $t_p = 0.16$.

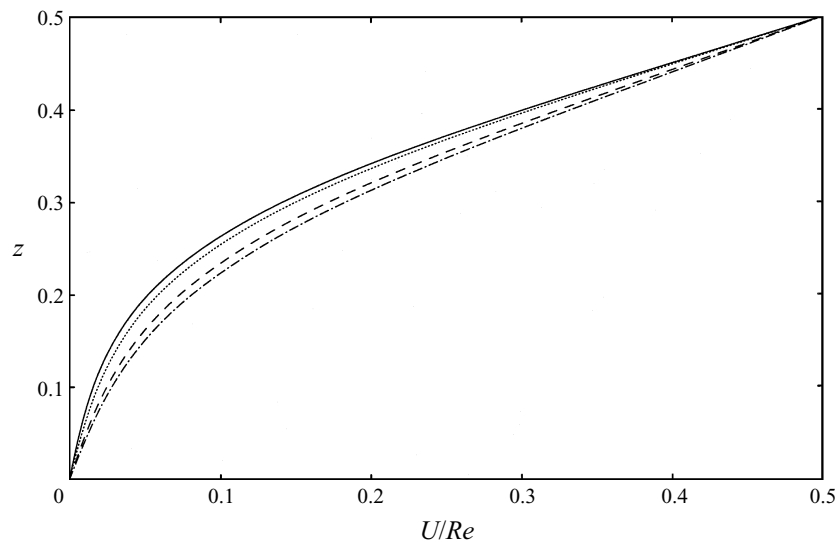


FIGURE 9. Profiles of the mean velocity, $U(z)$, in the x -direction in the case of oscillatory wavy rolls with $\alpha_x = 1.0, \alpha_y = 3.0, Re = 720$ at the times $t = 0$ (solid line), $t_p/4$ (dashed), $t_p/2$ (dotted), and $3t_p/4$ (dash-dotted) where the period is given by $t_p = 0.342$. This period includes two maxima of E_{pot} similarly to the case $Re = 630$ in figure 7(a).

also assumes an asymmetric shape which for the type of ATW solutions of figure 10 assumes the form shown in figure 11.

Because the ATW solution is steady with respect to a moving frame of reference, the coefficients in (5) are time independent with respect to the moving system and can be determined through a Newton–Raphson iteration. The momentum transport of the ATW is less than that of the wavy rolls as is apparent from the shear Nusselt

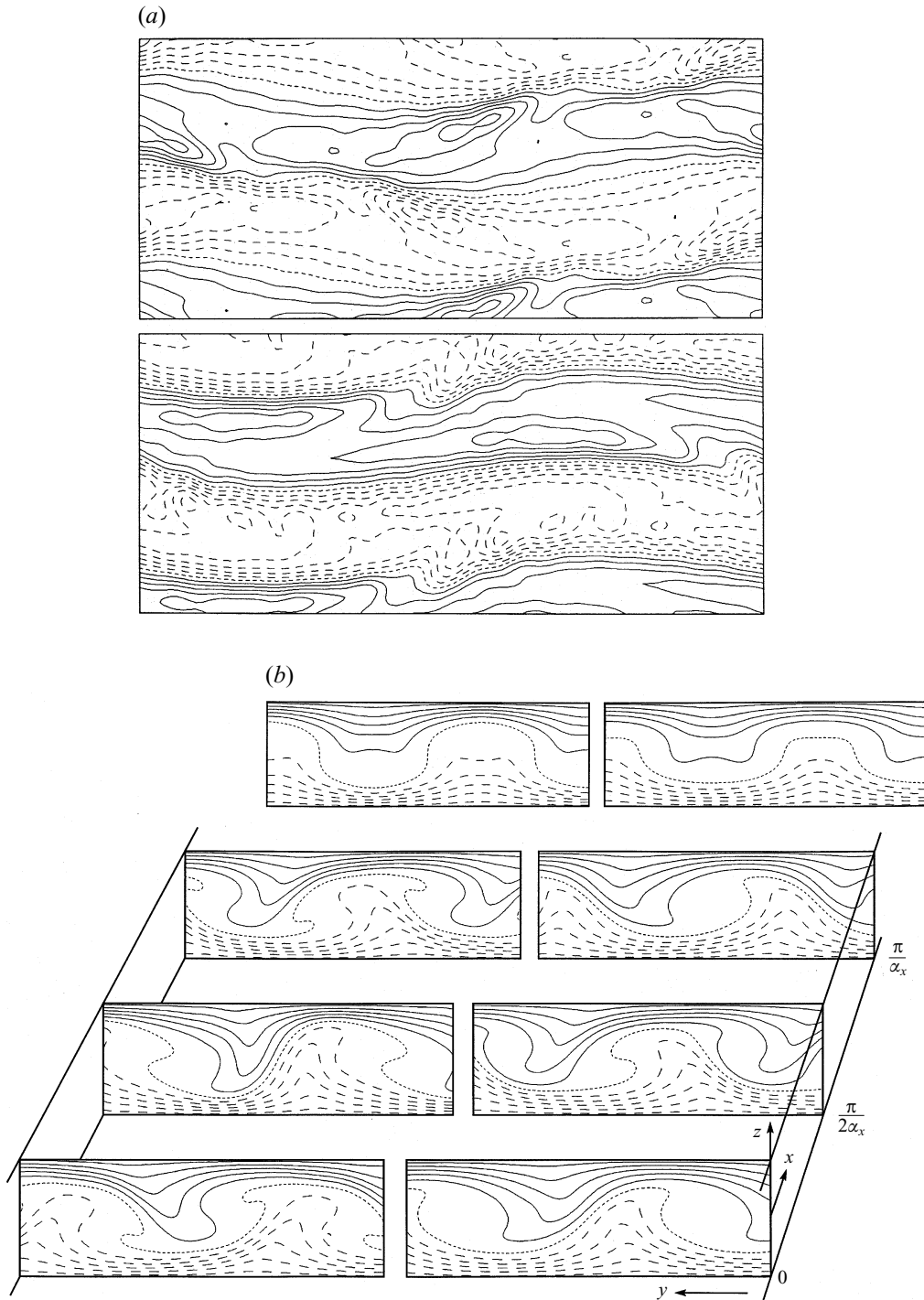


FIGURE 10. (a) Lines of constant z -velocity in the plane $z = 0$ for steady wavy rolls (upper plot) and asymmetric travelling waves (ATW) for $Re = 850, \alpha_x = 0.9, \alpha_y = 3.0$. $N_T = 18$ has been used for the solutions. The ATW travels in the positive x -direction (from left to right). (b) Lines of constant x -velocity in the planes $x = 0, x = \pi/2\alpha_x, x = \pi/\alpha_x$ as indicated and lines of constant x -average of the x -velocity (upper plots) for the steady wavy rolls (left plots) and for the ATW solution (right plots) in the same case as (a).

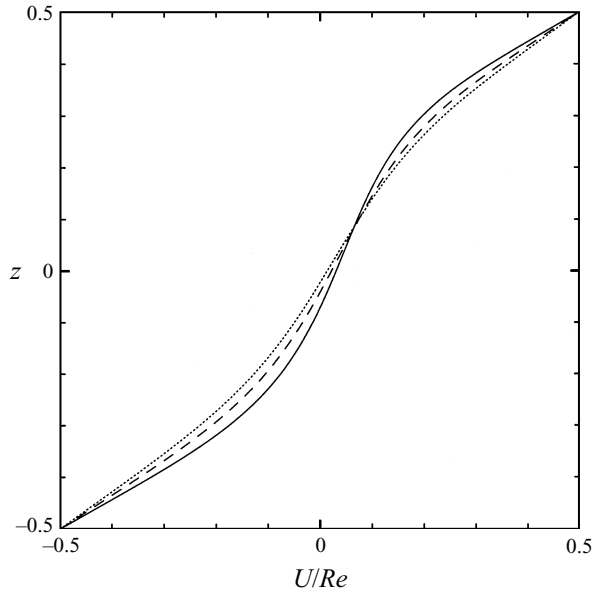


FIGURE 11. Profile of the mean flow for ATW solutions with $\alpha_x = 0.9, \alpha_y = 3.0$ and $Re = 750$ (dotted line), 850 (dashed line), and 1000 (solid line).

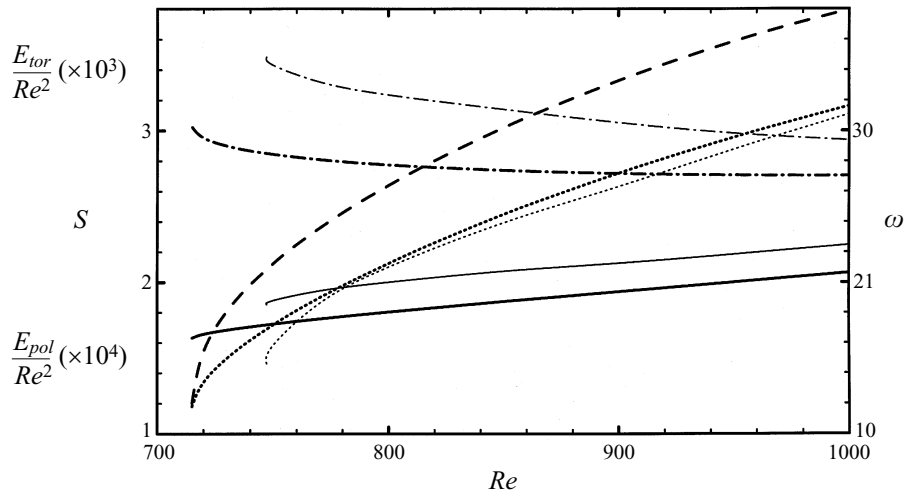


FIGURE 12. Shear Nusselt number S (solid lines), E_{pol} (dotted lines), and E_{tor} (dash-dotted lines) are shown for steady wavy rolls (thin lines) and ATW solutions (thick lines) as function of Re in the case $\alpha_x = 0.9, \alpha_y = 3.0$. Also shown is the frequency of the ATW solution (dashed line, right ordinate).

number plotted in figure 12 even though the poloidal component of the energy, E_{pol} , is higher. The toroidal component of the kinetic energy of the ATW is less than that of the wavy rolls and the distortion of the plane Couette flow profile is weaker such that the kinetic energy of the mean flow is higher. The frequency ω decreases rapidly towards an apparent saddle node which could be reached with the numerical scheme and ω may vanish at the yet unknown point of bifurcation from the steady wavy roll solution. There is thus not necessarily a contradiction between the vanishing

imaginary part of the growth rate of the AS -disturbances and the travelling wave solution to which they evolve.

5. Discussion

It is remarkable that the tertiary and quaternary solutions discussed in this paper exist at Reynolds numbers less than half the Reynolds number of 1440 at which sustained turbulence can be observed in experiments (Tillmark & Alfredsson 1992). The existence of nearly two-dimensional longitudinal vortices as tertiary solutions has stimulated experimenters to search for realizations of such solutions. By using a thin wire stretched in the spanwise direction of a plane Couette system Dauchot & Daviaud (1995) and more recently Bottin, Dauchot & Daviaud (1996) have demonstrated the excitation of longitudinal vortices. Although the minimum Reynolds number in the experiment depends somewhat on the thickness of the wire that is used for the generation of the longitudinal vortices, the lowest Reynolds numbers are typically of the order 600 as in the case of the theoretical solutions presented in this paper. A detailed comparison with the experimental measurements is difficult, however, because the periodicity of the vortices in the spanwise direction is usually not well established and there are no observations available of periods of oscillations.

The stability analysis that has been performed in §4 is far from general, of course, since the x, y -periodicity of the steady solution has been imposed onto the disturbances. Long-wavelength modulations of the vortex pattern are likely to occur which may lead to the turbulent spots that have typically been observed in large-scale numerical simulations (Lundbladh & Johansson 1991) as well as in laboratory experiments (see, for example, Tillmark & Alfredsson 1992). Nevertheless the observations as well as more recent simulations with smaller aspect ratio (Bech *et al.*, 1995; Hamilton, Kim & Waleffe 1995) show nearly periodic longitudinal roll vortices similar to those visualized in various figures of this paper (and a few additional ones shown in an earlier note, Busse & Clever 1996).

Most closely related to the analysis of the present paper are the numerical simulations of turbulent Couette flow by Hamilton *et al.* (1965). They use a relatively small periodicity interval in the plane parallel to the boundaries corresponding to $\alpha_x \approx 2.3$ and $\alpha_y = 3.4$ of the present analysis. But since their Reynolds number, set at 1600 according to the present scaling, is much beyond the range explored in preceding sections, their simulations show a turbulent flow. The finding of Hamilton *et al.* that the flow decays to the state of pure Couette flow when the periodicity interval is decreased agrees roughly with the present result that no solution can be obtained when α_y exceeds the critical value for a given value of α_x and vice versa. For example the maximum value of $\alpha_y \approx 4.3$ for $\alpha_x = 1.2$ at $Re = 1000$ is found according to figure 4(a) and this maximum value will decrease to 2.5 as α_x is increased to about 1.7 according to figure 5.

The fact that a special technique is needed at low Reynolds numbers for the experimental excitation of nearly longitudinal vortices indicates that these types of solutions have a small basin of attraction. This property is also evident from the numerical simulations. Time integrations have usually led to the trivial solution $\varphi \equiv \psi \equiv 0$ corresponding to plane Couette flow. Just as the steady solutions could only be obtained by changing the parameters in small steps, the time-dependent solutions have required the superposition of sufficiently small disturbances onto the steady solutions as an initial condition for the forward integration in time. Perhaps

future experimental developments will lead to a more direct realization of the tertiary and quaternary solutions discussed in this paper.

The research reported in this paper has been supported by the US National Science Foundation under Grant ATM-9417864 and by a NATO travel grant.

REFERENCES

- BECH, K. H., TILLMARK, N., ALFREDSSON, P. H. & ANDERSSON, H. I. 1995 An investigation of turbulent plane Couette flow at low Reynolds numbers. *J. Fluid Mech.* **286**, 291–325.
- BOTTIN, S., DAUCHOT, D. & DAVIAUD, F. 1996 Transition to turbulence in plane Couette flow: The streamwise vortices role. *J. Fluid Mech.* submitted.
- BUSSE, F. H. & CLEVER, R. M. 1996 Bifurcation sequences in problems of thermal convection and of plane Couette flow. In *Waves and Nonlinear Processes in Hydrodynamics* (ed. J. Grue, B. Gjevik & J. E. Weber), pp. 209–226. Kluwer.
- CHANDRASEKHAR, S. 1961 *Hydrodynamic and Hydromagnetic Stability*. Clarendon.
- CHERHABILI, A. & EHRENSTEIN, U. 1995 Spatially localized two-dimensional finite-amplitude states in plane Couette flow. *Eur. J. Mech. B/ Fluids* **14**, 677–696.
- CHERHABILI, A. & EHRENSTEIN, U. 1996 Existence and stability of finite-amplitude states in plane Couette flow. In *Advances in Turbulence VI, Proc. 6th European Turbulence Conf.* (ed. S. Gavrilakis, L. Machiels & P. A. Monkewitz), pp. 317–320. Kluwer.
- CLEVER, R. M. & BUSSE, F. H. 1992 Three-dimensional convection in a horizontal fluid layer subjected to a constant shear. *J. Fluid Mech.* **234**, 511–527.
- DAUCHOT, D. & DAVIAUD, F. 1995 Streamwise vortices in plane Couette flow. *Phys. Fluids* **7**, 901–903.
- HAMILTON, J. M., KIM, J. & WALEFFE, F. 1995 Regeneration mechanism of near-wall turbulence structures. *J. Fluid Mech.* **287**, 317–348.
- LUNDBLADH, A. & JOHANSSON, A. V. 1991 Direct simulation of turbulent spots in plane Couette flow. *J. Fluid Mech.* **229**, 499–516.
- NAGATA, M. 1988 On wavy instabilities of the Taylor-vortex flow between corotating cylinders. *J. Fluid Mech.* **188**, 585–598.
- NAGATA, M. 1990 Three-dimensional finite-amplitude solutions in plane Couette flow: bifurcation from infinity. *J. Fluid Mech.* **217**, 519–527.
- NAGATA, M. 1993 Stability of non-axisymmetric flows in the Taylor-Couette system. In *Unstable and Turbulent Motion of Fluid* (ed. S. Kida), pp. 3–9. World Scientific.
- TILLMARK, N. & ALFREDSSON, P. H. 1992 Experiments on transition in plane Couette flow. *J. Fluid Mech.* **235**, 89–102.